Biophysical Journal Volume 66 April 1994 978–988

A Model of the Electrophysiological Properties of Nucleus Reticularis Thalami Neurons

Gene V. Wallenstein
Program in Complex Systems and Brain Sciences, Center for Complex Systems, Florida Atlantic University, Boca Raton, Florida 33431 USA

ABSTRACT A model of the electrophysiological properties of rodent nucleus reticularis thalami (NRT) neurons of the dorsal lateral thalamus was developed using Hodgkin-Huxley style equations. The model incorporated voltage-dependent rate constants and kinetics obtained from recent voltage-clamp experiments in vitro. The intrinsic electroresponsivity of the model cell was found to be similar to several empirical observations. Three distinct modes of oscillatory activity were identified: 1) a pattern of slow rhythmic burst firing (0.5–7 Hz) usually associated with membrane potentials negative to approximately −70 mV which resulted from the interplay of I_{Ts} and $I_{K(Ca)}$; 2) at membrane potentials from approximately −69 to −62 mV, rhythmic burst firing in the spindle frequency range (7–12 Hz) developed and was immediately followed by a tonic tail of single spike firing after several bursts. The initial bursting rhythm resulted from the interaction of I_{Ts} and $I_{K(Ca)}$, with a slow after-depolarization due to I_{CAN} which mediated the later tonic firing; 3) with further depolarization of the membrane potential positive to approximately −61 mV, sustained tonic firing appeared in the 10–200-Hz frequency range depending on the amplitude of the injected current. The frequency of this firing was also dependent on the maximum conductance of the leak current, $I_{K(leak)}$, and an interaction between the fast currents involved in generating action potentials, $I_{Na(fast)}$ and $I_{K(DR)}$, and the persistent Na^+ current, $I_{Na(P)}$. Transitions between different firing modes were identified and studied parametrically.

INTRODUCTION

It has been known since the 1940s that cortical spindle rhythms (7–14 Hz) observed during periods of decreased vigilance (drowsiness and sleep) are generated in the thalamus (Morison and Basset, 1945). Other types of cortical oscillations such as the delta rhythm (0.5–4 Hz) which accompanies slow wave sleep have been thought to originate cortically (e.g., Steriade et al., 1990), but recent in vivo (Nuñez et al., 1992) and in vitro (Bal and McCormick, 1993) studies suggest that both modes of oscillatory activity may have a common cellular basis in the dorsal lateral thalamus. For example, Steriade et al. (1986) have suggested that spindle rhythmicity is generated specifically in the nucleus reticularis thalami (NRT) which has reciprocal connections with thalamocortical relay (TCR) neurons of the dorsal lateral thalamus. Evidence in favor of this hypothesis includes: 1) the fact that when the reticular thalamic nucleus is surgically isolated, it is still capable of generating spindles whereas other thalamic groups including those afferent to the cortex are not (Steriade et al., 1987); 2) neurons of the anterior thalamic nuclei and habenula which are naturally devoid of input from the reticular thalamic nucleus do not display spindles in vivo (Steriade et al., 1987) and; 3) the discovery of low-threshold Ca^{2+} channels which allow bursting behavior in NRT and TCR cells following their release from hyperpolarization (Jahnsen and Llinás, 1984a, b). The third point is crucial because the discovery of reciprocal dendrodendritic synapses among NRT cells may provide a structural basis for spindle generation (Deschênes et al., 1985).

In many ways, the NRT is ideally suited to foster intrathalamic rhythmicity. It receives collaterals from both thalamocortical and corticothalamic fibers (Harris, 1987) and projects divergently to TCR cells of the dorsal thalamus (e.g., Steriade and Llinás, 1988). It has been observed that GABAergic inhibition from NRT neurons can hyperpolarize target TCR cells sufficiently to deinactivate the transient T-type Ca^{2+} current which underlies postinhibitory low-threshold bursting (Wallenstein, submitted for publication; Crunelli and Leresche, 1991). TCR cells can then excite NRT neurons synaptically through a glutamate-activated cation current which may lead to reverberatory oscillations (see Steriade et al. (1990)). Furthermore, the NRT is innervated noradrenergically by fibers from the locus coeruleus (Asanuma, 1992), cholinergically from the brainstem and basal forebrain groups CH5 and CH6 (Asanuma, 1989; Hallanger et al., 1987), and serotonergically from the raphe nucleus (Lavoie and Parent, 1991). Acetylcholine has a powerful inhibitory influence on NRT cells by increasing a muscarinic M_2-receptor mediated K^+ current (McCormick and Prince, 1986), while applications of noradrenaline excite these cells through an α_1-adrenoceptor-coupled decrease in G_K (McCormick and Prince, 1988), thus providing an additional means by which to shape the oscillatory behavior of the NRT-TCR circuit.

Recent voltage-clamp experiments have begun to establish the ionic basis for these and other electrophysiological responses demonstrated in NRT cells in vitro (Avanzini et al., 1989; Huguenard and Prince, 1992; Bal and McCormick,

Received for publication 22 October 1993 and in final form 10 January 1994.

Address reprint requests to Gene V. Wallenstein, Center for Complex Systems and Brain Sciences, Florida Atlantic University, Boca Raton, FL 33431 USA. Tel.: 407-367-2230; Fax: 407-367-3634; E-mail: wallenstein@walt.ccs.fau.edu.

0006-3495/94/04/978/11 $2.00

1993). In particular, Bal and McCormick (1993) have identified three distinct modes of activity in NRT neurons including 0.5–7 Hz rhythmic bursting at membrane potentials, V, negative to −70 mV, spindle rhythms at slightly more depolarized values (approximately −69 to −62 mV), and tonic single spike firing from 10–200 Hz at V positive to −60 mV, the latter being linearly dependent on the amplitude of the injected current. In what follows, we present a theoretical model of a single NRT neuron incorporating the intrinsic ionic currents known to contribute to these phenomena and elucidate the manner in which their interaction generates this behavior. The model is shown to exhibit all three firing modes observed in vitro, including a nearly linear relationship between tonic firing frequency and injected current (Bal and McCormick, 1993). Furthermore, transitions between different firing modes were studied parametrically and found to be consistent with these empirical results (Bal and McCormick, 1993). Finally, the modulatory role of ascending synaptic input is examined with regard to the influence it has on these firing states. In particular, it is shown that modulation by partially occluding the leakage current, $I_{K(leak)}$, directly influences firing frequency of the cell within each mode.

STRUCTURE OF THE MODEL

The ionic currents of the NRT cell were modeled with Hodgkin-Huxley type equations (Hodgkin and Huxley, 1952). To reproduce the properties of NRT neurons discussed above, a "point" (single compartment) model neuron was composed of ten currents which included $I_{Na(fast)}$, $I_{K(DR)}$, I_{Ts}, I_L, $I_{K(Ca)}$, I_{CAN}, $I_{Na(P)}$, $I_{K(A)}$, $I_{Na(leak)}$, and $I_{K(leak)}$. Since the primary motivation behind this work is to understand the oscillatory phenomena believed to be intrinsic to NRT cells (Bal and McCormick, 1993), synaptic currents have been omitted in these simulations.[1]

The principal equation describing the change in voltage potential of the neuron is given by

$$C_m\dot{V} = -I_{Na(fast)} - I_{K(DR)} - I_{Ts} - I_L - I_{K(Ca)} - I_{CAN} - I_{Na(P)} - I_{K(A)} - I_{Na(leak)} - I_{K(leak)}, \quad (1)$$

where C_m, the input capacitance, is equal to 0.242 nF assuming a total membrane area of 24,200 μm^2 (Mulle et al., 1986), and specific membrane capacitance of 1 $\mu F/cm^2$. The general form governing the change in current is a simple extension of Ohm's law,

$$I_{ion} = \bar{g}_{ion} m^n h (V - V_{ion}) \quad (2)$$

where $\bar{g}_{ion}$ is the maximal conductance for this ion, V_{ion} is the reversal potential, and m and h are activation and inactivation constants, respectively. The constants follow first order reaction kinetics of the form

$$1 - m \underset{\beta_m}{\overset{\alpha_m}{\rightleftharpoons}} m. \quad (3)$$

In this case, m may be thought of as the probability of a membrane-bound particle being in the correct position to gate the channel open (Hodgkin and Huxley, 1952). The transition between "nonpermissive" $(1 - m)$ and "permissive" states is governed by the forward and backward rate constants, α_m and β_m, respectively. These rate constants can be dependent on membrane potential, V, or the internal concentration of a particular ion (e.g., $I_{K(Ca)}$ and I_{CAN}). Once the rate functions are known, the time-dependent values of the (in)activation variable can be calculated by solving,

$$\dot{m} = (m_\infty - m)/\tau_m, \quad (4)$$

where

$$m_\infty = \alpha_m/(\alpha_m + \beta_m) \quad (5)$$

$$\tau_m = 1/(\alpha_m + \beta_m). \quad (6)$$

For each of the currents utilized in these simulations, the rate constants were derived directly from recent empirical observations reported in the literature and the temperature was set at 35°C. Unless otherwise stated, the kinetics of each current were assumed to have a Q_{10} of 3 (see Appendix for details). We now present some justification and comments for their inclusion in the model.

1 and 2) *$I_{Na(fast)}$ and $I_{K(DR)}$*—Both the fast transient Na^+ and delayed rectifier K^+ currents are central in generating action potentials in NRT neurons (Avanzini et al., 1989; Bal and McCormick, 1993). The forward and backward rate constants for both of these currents have previously been modeled by McCormick and Huguenard (1992) based on data obtained from cortical pyramidal cells (Huguenard et al., 1988). We have used these functions in the simulations reported here.

3) *I_{Ts}*—It was reported recently that the transition from tonic to burst firing in NRT neurons is mediated by the deinactivation of a slow Ca^{2+} current which underlies low-threshold Ca^{2+} potentials (Huguenard and Prince, 1992). This transient inward current is deinactivated by prolonged hyperpolarization similarly to I_T in TCR cells, however, the voltage dependence of activation is slightly more depolarized ($V_{1/2}$ = −43 mV). Additionally, the rate of activation is much slower than I_T, while the inactivation rate was found to be voltage independent in these cells (Huguenard and Prince, 1992). To model this current we utilized the activation and inactivation parameters reported by Huguenard and Prince (1992) and fitted equations to their reported kinetic data (Fig. 6 *c* and 6 *d* in Huguenard and Prince (1992)).

[1] A recent model was developed by Destexhe et al. (1993) of 8–10-Hz spindle oscillations using synaptically connected NRT and thalamocortical relay cells. Since the goal of their model was to "...find the minimal number of ionic mechanisms that account for spindling," not all the ionic currents known to exist in these cells were included. Our purpose here is to model both bursting as well as *single spike firing properties* and the *transitions between various firing states* believed to be intrinsic to NRT neurons. It is shown in later sections that in order to account for these experimental observations, several additional currents are required. Consequently, the model presented here contains all the intrinsic currents known to contribute to the electroresponsive properties of NRT cells, but no synaptic mechanisms.

4) I_L—In addition to I_{Ts}, the existence of a high-threshold Ca^{2+} current in NRT neurons similar to that observed in TCR cells has been postulated (Bal and McCormick, 1993). Intracellular recordings from TCR cells in vitro have revealed that both fast action potentials and high-threshold spikes are followed by a marked increase in Ca^{2+}-dependent K^+ currents, while low-threshold potentials are not (Jahnsen and Llinás, 1984a, b). Since NRT neurons have a substantial after-hyperpolarization (AHP) which contributes to the intrinsic rhythmicity of bursting in the cell, it is likely that additional entry of Ca^{2+} into the cell such as that from I_L helps mediate the AHP following the burst response. Since rate functions of this current have yet to be derived for TCR cells, we employed the activation equations given by Kay and Wong (1987).

5) $I_{K(Ca)}$—Intracellular recordings from NRT cells in vitro have demonstrated that the primary current underlying the burst AHP is $I_{K(Ca)}$ (Avanzini et al., 1989; Bal and McCormick, 1993). Examination of the burst AHP showed it to be sensitive to both the K^+-channel blocker $C3^+$ and bath application of TEA, and have a reversal potential closely matching that of K^+ (Bal and McCormick, 1993). Because I_L is activated during the burst response of fast action potentials, an increase in $I_{K(Ca)}$ serves to repolarize the cell in between bursts. The amplitude and duration of the AHP in conjunction with I_{Ts}, thus determines the frequency of rhythmical bursting. To account for this current in our model we used the equations of Yamada et al. (1989) derived originally from frog sympathetic ganglion cells, but modified by Destexhe et al. (1993) to fit data from intracellular recordings of NRT cells in vitro.

6) I_{CAN}—In addition to the burst AHP of NRT cells observed in vitro, Bal and McCormick (1993) have also demonstrated the presence of a slow burst after-depolarization (ADP). They found the ADP could be supported by $choline^+$, but not *N*-methyl-D-$glucamine^+$, and that neither affected the low-threshold Ca^{2+} potential, thus suggesting that the response is mediated by a Ca^{2+}-activated nonspecific cation current, I_{CAN} (Bal and McCormick, 1993; see Partridge and Swandulla (1988), for a review). It appears that I_{CAN} may play a critical role in modulating the duration of rhythmical bursting and contribute to the appearance of the single spike firing which typically follows the termination of such oscillatory behavior within the spindle frequency range (Bal and McCormick, 1993). Similar to $I_{K(Ca)}$, we used modifications to the equations of Yamada et al. (1989) developed by Destexhe et al. (1993) to model I_{CAN} in NRT neurons.

7) $I_{Na(P)}$—Intracellular recordings of NRT neurons in vitro have demonstrated that a persistent Na^+ current contributes substantially to the firing frequency during the tonic, single spike firing mode (Bal and McCormick, 1993). Application of tetrodotoxin during tonic firing reportedly abolished all action potentials and hyperpolarized the membrane potential by 5–6 mV (Bal and McCormick, 1993). At present, the kinetics of activation of this current are not yet available, however, the voltage dependence of activation can be modeled in accordance with data obtained from hippocampal pyramidal cells (French et al., 1990).

8) $I_{K(A)}$—Recent intracellular recordings in NRT cells in vitro have noted that the burst AHP is composed primarily of K^+ currents (Avanzini et al., 1989; Bal and McCormick, 1993). When rodent NRT neurons are briefly hyperpolarized from rest ($V_{rest} \approx -68$ mV), a series of slow rhythmical bursts occur in the 0.5–7-Hz frequency range. When hyperpolarized from potentials in the range from approximately V_{rest} to -61 mV, the frequency of rhythmical bursting increases and is followed by a gradual shift from burst to single spike firing with the latter becoming prominent at more depolarized values of V (Fig. 3 *a* in Bal and McCormick (1993)). During this period of single spike firing, NRT cells can sometimes exhibit considerable spike-frequency adaptation (Bal and McCormick, 1993). Although the underlying current(s) producing this phenomenon have yet to be addressed in detail in NRT neurons, we postulate that a similar mechanism as that which operates in TCR cells may be active in these GABAergic groups (Huguenard et al., 1991). Huguenard and McCormick (1992) have recently derived a model of this current and we have incorporated it into our model cell.

9, 10) $I_{Na(leak)}$ *and* $K_{K(leak)}$—The remaining Na^+ and K^+ leakage currents were set with a maximal conductance such that the resting potential of the NRT cell was consistent with values reported in the literature (Appendix).

RESULTS

Slow (1–7 Hz) rhythmical bursting

As mentioned above, when NRT cells are injected with a hyperpolarizing current at membrane potentials negative to approximately V_{rest}, a rebound sequence of slow rhythmical bursts occurs with an interburst frequency from 1–7 Hz (Bal and McCormick, 1993). In Fig. 1, we show a typical example of slow bursting in the model neuron. In this instance, a hyperpolarizing current was injected for 100 ms at -68 mV, which results in a sequence of two bursts at approximately 6 Hz. This slow bursting is the result of an interplay between primarily two currents, I_{Ts} and $I_{K(Ca)}$. On release from hyperpolarization, I_{Ts} becomes deinactivated and begins entering the cell which in turn triggers a subsequent increase in $I_{K(Ca)}$ and the slow Ca^{2+}-dependent nonspecific cation current, I_{CAN}. Because of the substantial size of $I_{K(Ca)}$ ($\approx$10 nA in this example), a prolonged burst AHP is produced which is of sufficient amplitude and duration to deinactivate I_{Ts} once again and produce another Ca^{2+}-dependent burst. This cycle is then broken after the reduction in $I_{K(Ca)}$ (and previous reduction in I_{Ts}) fails to hyperpolarize the cell long enough to produce a third response in I_{Ts}, however, there is a small increase in V where the next response would appear given an increase in conductance. These simulated observations, including the overall appearance of the burst, are consistent with recent experimental results demonstrated in guinea pig NRT neurons in vitro (Bal and McCormick, 1993).

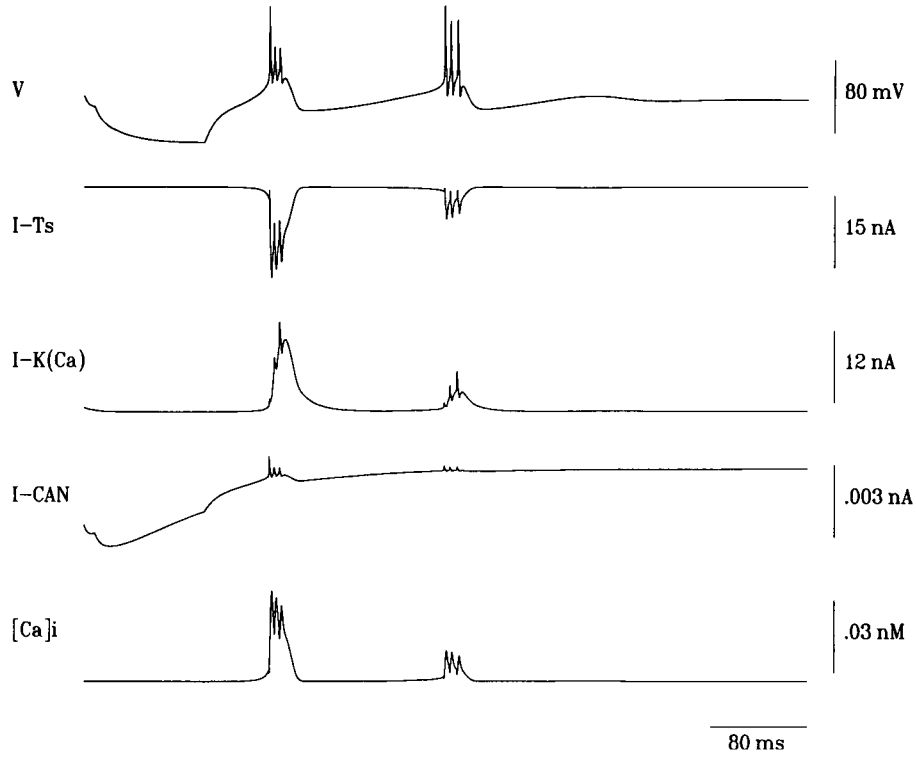

FIGURE 1 An example of slow rhythmical burst firing (6 Hz). A hyperpolarizing current of −0.4 nA was injected for 120 ms, resulting in a rebound oscillation of *V*. Also shown are the primary currents involved in slow bursting, I_{Ts}, $I_{K(Ca)}$, I_{CAN}, and the time-dependent changes in intracellular calcium concentration. Typically, slow bursting consisted of only two to three burst events before dying out.

Spindle rhythms (7–14 Hz)

Thalamic spindle rhythms accompanying synchronized EEG are rhythmic burst oscillations grouped in sequences that last for approximately 1–2 s and recur every 5–10 s (Steriade et al., 1990). This characteristic waxing and waning nature of these oscillations has been observed in both in vitro (von Krosigk et al., 1993) and in vivo (Mulle et al., 1986) preparations. Recent in vitro recordings made from rodent NRT neurons have demonstrated rhythmical burst oscillations in the spindle frequency range following a brief hyperpolarizing current injection (Avanzini et al., 1989; Bal and McCormick, 1993). In such instances, a series of 5–10 low-threshold Ca^{2+}-dependent bursts occur in the frequency range of spindle oscillations and gradually subside as one or more single action potentials fire (See Fig. 2 *a* in Avanzini et al. (1992) or Fig. 3 *a* in Bal and McCormick (1993)). In Fig. 2 *A*, we illustrate this property by subjecting the model NRT cell to a brief hyperpolarizing current of 120-ms duration at −64 mV. The same gradual shift from burst firing to single spike mode observed in vitro is exhibited by the model cell. The rhythmical bursting has a frequency of recurrence at approximately 10 Hz and terminates after roughly 1.25 s, which is consistent with empirical results (Avanzini et al., 1989; Bal and McCormick, 1993) as well as a theoretical model of spindle rhythms in interconnected TCR and NRT cells (Destexhe et al., 1993). When the same hyperpolarizing current was injected into the cell at −59 mV (Fig. 2 *B*), the interburst frequency increased to approximately 14 Hz and after shifting into single spike firing remained there for a longer duration. This property has also been observed in NRT cells under similar conditions in vitro (Bal and McCormick, 1993).

The rhythmical bursting portion of these data is essentially the result of the same interacting currents as that demonstrated for slower bursting, namely I_{Ts} and $I_{K(Ca)}$. The switch to single spike firing at the tail end of the burst sequence is due to the increase in I_{CAN}, which has a slow ramp-like appearance that reaches maximum at the same instant as the switching time. As I_{CAN} reaches its maximum (marked by the *arrow* in Fig. 2 *B*), both I_{Ts} and $I_{K(Ca)}$ achieve their respective minimal values at the same moment. This is demonstrated in Fig. 2 *B*, where the increase in I_{CAN} (≈2 nA) is observable along with subsequent decreases in both I_{Ts} and $I_{K(Ca)}$. Once the single spike firing begins, it is sustained for a short duration by the persistent Na^+ current, which is also active during bursting. When $I_{Na(P)}$ was eliminated from the model, single spike firing following the burst sequence terminated after only one or two spike events, resembling the activity shown in Fig. 2 *A*. The increase in interburst frequency observed when the model cell was injected at $V = -59$ mV, stems from the increase in the rate of activation in I_{Ts} (τ_m in the Appendix) at *V* positive to −60 mV (Huguenard and Prince, 1992). In the present model, τ_m has its slowest value at −63 mV.

Frequency modulation of single spike firing

Bal and McCormick (1993) demonstrated that when a rodent NRT cell is injected with a constant depolarizing current pulse at *V* slightly more positive than −60 mV, a sequence of sustained single spikes fire in the frequency range from

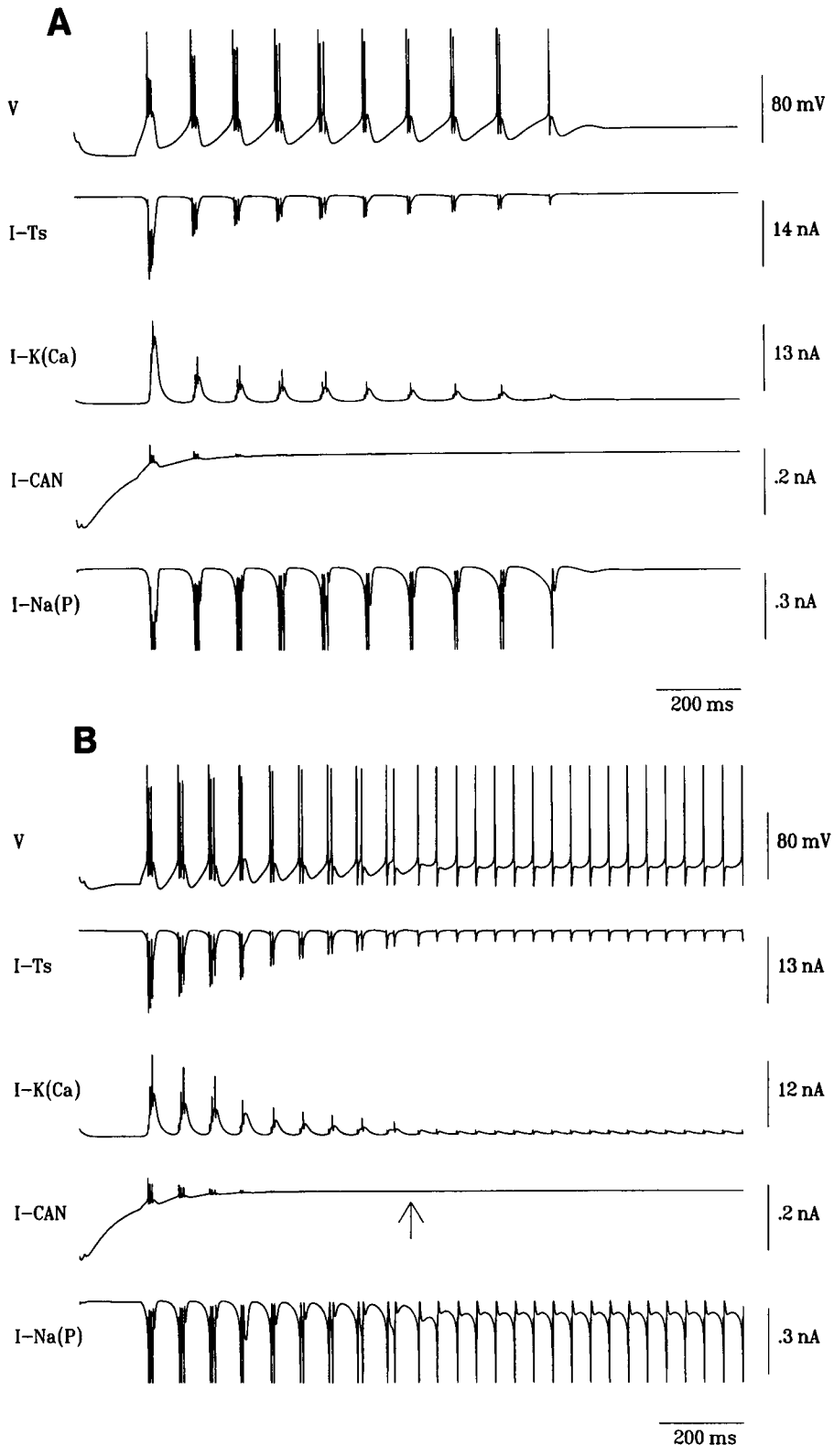

FIGURE 2 (*A*) A sequence of repetitive burst firing in the spindle rhythm frequency range (7–14 Hz), terminating in a single action potential. Also shown are the primary currents involved in the generation of spindle rhythms in NRT cells (see text). The cell was injected with a hyperpolarizing current of −0.2 nA for 120 ms at −64 mV. (*B*) Same as in *a*, however, the cell was initiated at −59 mV prior to the current injection. This results in a longer lasting tail of single spike firing following the burst sequence. The arrow indicates when the maximum in I_{CAN} is first attained.

approximately 10 − 400 Hz in vitro depending on the amplitude of the injected current. Despite previous suggestions that NRT cells may have an intrinsic propensity toward firing in the 30–60-Hz range (Pinault and Deschênes, 1992), they observed an approximately linear relationship between injected current and firing frequency (Fig. 11 *d* in Bal and McCormick (1993)). In Fig. 3 *A*, the response of the model NRT cell to a constantly injected depolarizing current of 0.2 nA at −56 mV is shown. Once the firing reaches a steady-state, it maintains a consistent rhythm close to 80 Hz, which

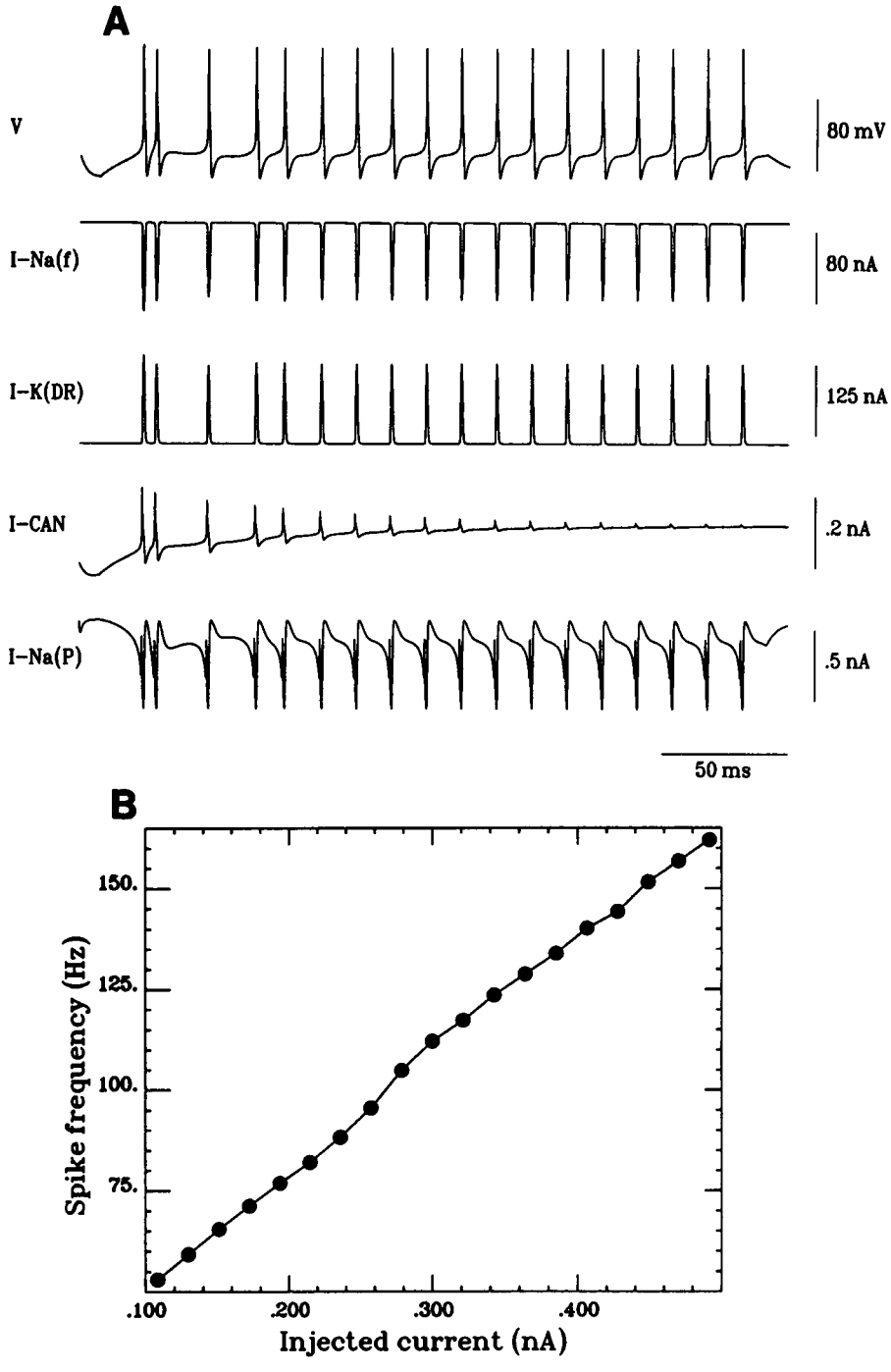

FIGURE 3 (*A*) An example of single spike firing in the NRT cell model. The cell was injected with a constant depolarizing current of 0.2 nA initiated at −56 mV, resulting in a sequence of fast action potentials at 80 Hz. Also shown are the currents underlying this response; the fast Na^+ and K^+ currents, the Ca^{2+}-dependent cation current, I_{CAN}, and the persistent Na^+ current. (*B*) Similar to NRT cells in vitro, the model displayed an approximately linear relationship between the amplitude of the injected current (at −56 mV) and the firing frequency in single spike mode.

is congruent with values reported in vitro under similar conditions (Bal and McCormick, 1993).

The primary currents underlying single spike firing in NRT cells are the fast Na^+ current, $I_{Na(fast)}$, the delayed rectifying K^+ current, $I_{K(DR)}$, the persistent Na^+ current, $I_{Na(P)}$, the K^+ current, $I_{K(A)}$ and the Ca^{2+}-dependent cation current, I_{CAN}. Once I_{CAN} reaches a constant value, the steady-state firing of single action potentials ensues. The frequency of firing in single spike mode depends on the balance between $I_{Na(P)}$ and $I_{K(Ca)}$. With increased depolarization from V_{rest}, $I_{Na(P)}$ activates and drives V toward the threshold for action potential generation more quickly. As $I_{Na(P)}$ increases, this causes a complimentary increase $I_{K(A)}$ thus affecting the time period between spikes. Similar to that which has been observed in vitro (compare with Fig. 11 *d* in Bal and McCormick (1993)), the model NRT cell displayed an approximately linear relationship between firing frequency and the amplitude of injected current (Fig. 3 *B*). When $I_{K(A)}$ was eliminated from the model the firing frequency nearly doubled for injected current (I_{inj}) values between 0.1 and 0.25 nA and by approximately 60% at 0.25 nA < I_{inj} < 0.3 nA (not shown).

Influence of I_{inj} and initial voltage on firing state

In addition to changing the frequency of firing in single spike mode, I_{inj} also influenced the firing state of the model cell. Typically, depolarizing currents administered over a wide range of initial voltages resulted in single spike firing (as shown in Fig. 3 *B*). However, hyperpolarizing currents yielded a variety of firing modes depending on the membrane potential at which the current was delivered (Fig. 4). Transitions from slow repetitive bursting to bursting in the spindle frequency range were possible through two different routes. For relatively small magnitudes of I_{inj} (e.g., -0.36 nA < I_{inj} < -0.05 nA), the switch from "slow" to "spindle" bursting is rather continuous with a gradual increase in frequency. However, there was a marked change in the number of bursts from two or three events during the slow oscillations to 8–15 bursts in the spindle frequency range.

The second route involved the sequence, "slow bursting," "slow bursting followed by a tail of single spikes," and "spindle bursting followed by a tail of single spikes" (Fig. 4). When the slow bursting was followed by single spikes, in general, only two or three ensued. However, as the transition to spindle oscillations occurred through this route, the bursting was followed by a range of single spikes from 1 to 16, with the highest number of spikes occurring at the most depolarized initial voltages (-50 mV in this case). This latter route from slow to spindle frequency bursting is consistent with recent in vitro observations in which a hyperpolarizing current of -0.5 nA was injected into the cell (Bal and McCormick, 1993).

Modulation of firing frequency by $I_{K(leak)}$

Because the firing frequency within the bursting and single spike mode of NRT cells is dependent on the membrane potential before and during stimulation, it is not surprising that leakage currents which affect these properties can also modulate firing activity. For example, it is known that application of either 5-HT or noradrenaline (McCormick and Prince, 1988; McCormick and Wang, 1991; Bal and McCormick, 1993) to NRT neurons in vitro results in a slow but sustained increase in the excitability of the cell. Recent intracellular recordings have suggested that the increase in excitability through application of noradrenaline might be due to an α_1-adrenoceptor-coupled decrease in $I_{K(leak)}$ (McCormick and Prince, 1988; McCormick, 1989).

In Fig. 5, we show the response of the model cell to gradual changes in the maximal conductance, *gl*, of $I_{K(leak)}$. In the top graph (Fig. 5 *A*), the cell was administered a constant depolarizing current of 0.1 nA. Clearly, the primary change to the firing pattern is in its frequency, which increases from approximately 15 Hz when $gl = 7$ nS to 120 Hz at $gl = 1$ nS. Similarly, when a brief hyperpolarizing current of 50 ms at -0.1 nA is injected into the cell (Fig. 5 *B*), the result is a doubling of the interburst frequency when *gl* is decreased over the same range. In both firing modes, when $gl = 9$ nS, there is simply too much K^+ leaving the cell through this passive channel, and it becomes hyperpolarized to the point where it fails to reach the threshold for firing. These results suggest that any synaptic currents known to affect $I_{K(leak)}$, can serve a modulatory role in the ongoing activity of these cells. Indeed, particularly in the case of single spike firing, it would seem that the excitatory glutamatergic input from thalamocortical relay cells could be modulated over a substantial frequency range simply by small changes in the amplitude of $I_{K(leak)}$.

DISCUSSION

By developing a model of nucleus reticularis thalami neurons using Hodgkin-Huxley type equations to characterize the voltage and time-dependent properties of the currents intrinsic to these cells, it has been possible to study the manner in which these currents interact during different firing modes. Similar to recent experimental observations in vitro, it was shown that three distinct modes of oscillatory activity are

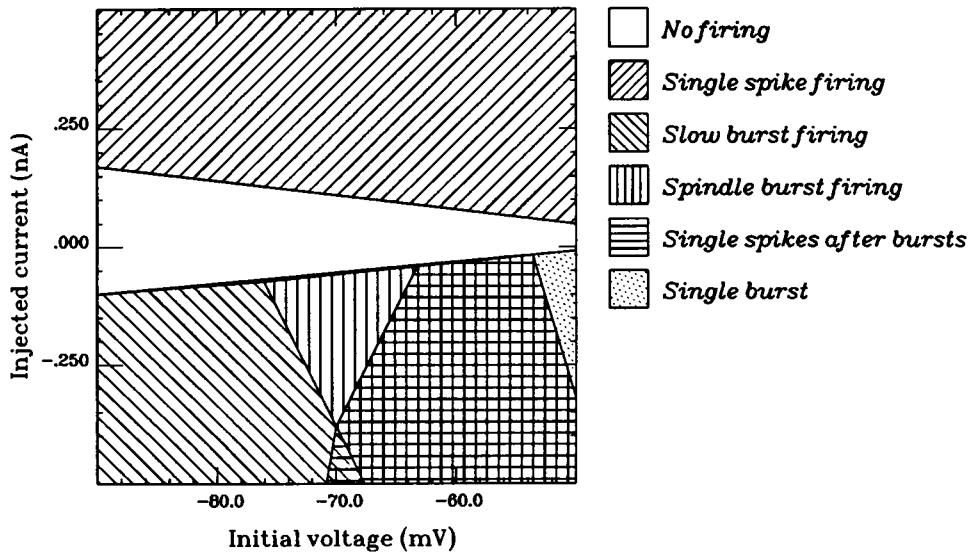

FIGURE 4 The influence of I_{inj} and initial voltage on the firing activity of the model. A current was injected for 150 ms over a wide range of I_{inj} magnitudes and initial voltages. Slow bursting at 1–7 Hz usually consisted of no more than two or three burst events, while bursting in the spindle frequency range (7–14 Hz) consisted of 8–15 events. Two routes from slow to spindle bursting were identified depending on the magnitude of I_{inj} (see text).

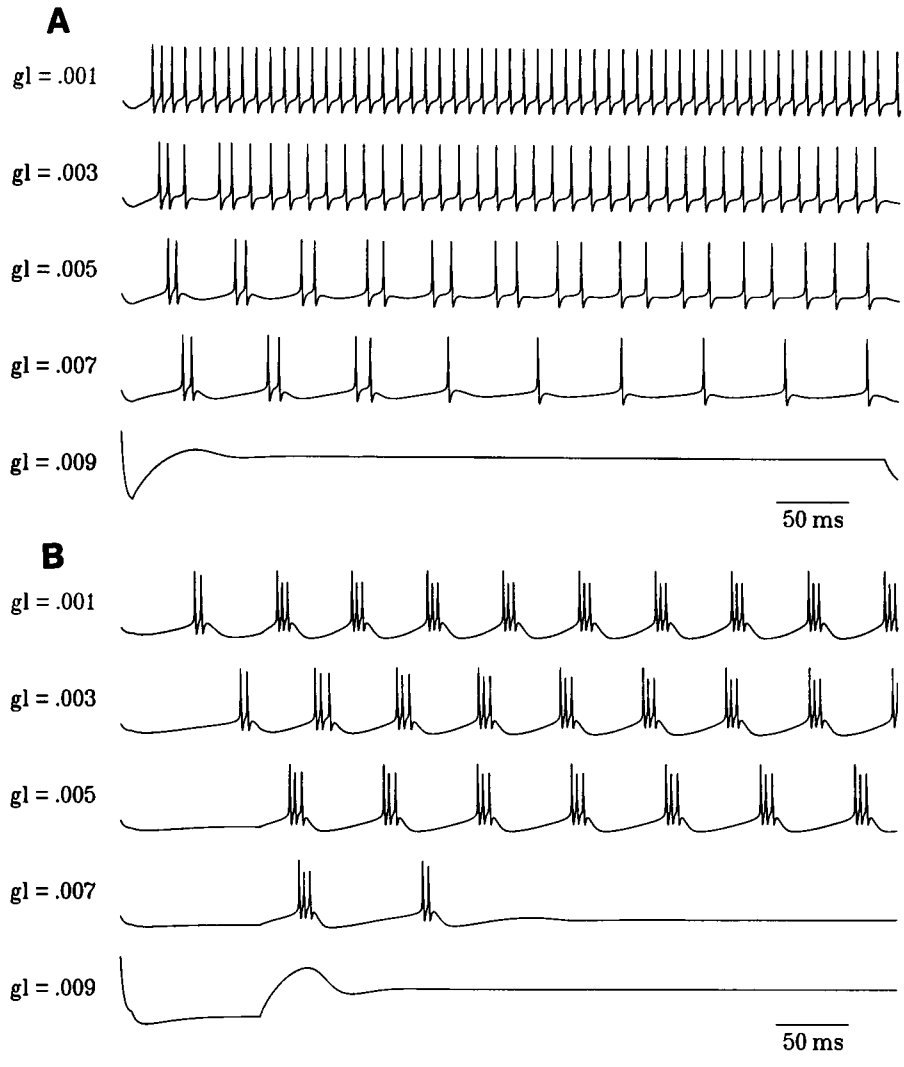

FIGURE 5 The influence of changing the maximum conductance, *gl*, of the K^+ leakage current, $I_{K(leak)}$. (*A*) The model was administered a constant depolarizing current of 0.1 nA, which results in a series of single spikes. By decreasing the conductance of $I_{K(leak)}$ from 7 to 1 nS, the frequency of firing increases by over 100 Hz. (*B*) An injection of a brief hyperpolarizing current of −0.1 nA for 50 ms into the cell, demonstrates that an increase (albeit smaller) in firing frequency also occurs in bursting mode when *gl* is decreased over the same range as in *A*.

possible in NRT cells (Bal and McCormick, 1993). Slow rhythmical bursting in the 1–7-Hz frequency range was observed for membrane potentials negative to −70 mV. Repetitive burst firing in the spindle rhythm frequency range was shown to occur at membrane potentials from approximately −69 mV to −62 mV. And finally, single spike firing was exhibited for *V* positive to −61 mV, the frequency of which was found to be linearly related to the amplitude of injected current.

The transition from slow to spindle frequency range bursting was parametrically explored as a function of I_{inj} and initial membrane voltage. Two different routes were observed. The route which included a tail of single spikes following both slow and spindle frequency bursting has recently been observed experimentally in vitro over approximately the same values of I_{inj} and initial voltage exhibited in the model. The other route must still be tested empirically by using smaller magnitudes of I_{inj}.

Because at present there is not sufficient information to characterize the density and spatial distribution of individual channels in these neurons, the currents were modelled macroscopically. However, by employing equations of NRT cell currents which were derived directly from intracellular patch-clamp investigations, the simulation proved effective in reproducing the overall structure of the individual burst and action potential as well as the oscillatory behavior of these neurons. Moreover, the model can also be used to understand how NRT cells contribute to ongoing "network" behavior. For example, it is known that the duration and slow recurrence (0.1–0.3 Hz) of thalamic spindle rhythms is shaped by both the endogenous electrophysiological properties of NRT and TCR cells as well as the nature of their interaction (McCormick, 1992a). An interesting feature observed in vitro in rodent NRT neurons (Avanzini et al., 1989; Bal and McCormick, 1993), and the model is the appearance of rhythmical bursts in the spindle frequency range which last for several cycles (5–15) and terminate as the Ca^{2+}-dependent cation current, I_{CAN} becomes larger and shunts both I_{Ts} and $I_{K(Ca)}$ (Fig. 2 *A*). Both the inter-burst frequency (7–14 Hz) and the duration (1–2 s) of this rhythmical behavior is consistent with thalamic spindling in vivo (Steriade and Deschênes, 1984; Steriade and Llinás, 1988). Considering the possible functional importance of NRT cells in generating these oscillations (Deschênes et al., 1985; Ste-

riade et al., 1987), such behavior may directly contribute to the waxing and waning character of thalamic spindles in vivo (but see Destexhe et al. (1993)). This possibility could be tested experimentally by pharmacologically altering I_{CAN} and observing the changes in both the duration and recurrence of spindle events.

In addition to the intrinsic currents represented in the model, NRT cells are directly modulated by several ascending groups synaptically. Neurotransmitters such as noradrenaline which have been shown to alter the conductance properties of the passive K^+ leakage current in thalamic cells (McCormick, 1989; 1992b) indirectly shape the firing frequency of NRT neurons by changing the overall resistivity of the cell. Indeed, the model predicted that decreases in the maximum conductance of $I_{K(leak)}$ on the order of 6 nS result in a 100-Hz increase in the frequency of single spike firing. Thus the role of even minute alterations to this current is likely to be substantial in shaping the level of activity of these cell groups in vivo and could be test experimentally in a quantitative manner.

When models such as this are incorporated with their full array of synaptic influences and interconnected with other groups in a topologically realistic manner they can assist us in our goal toward understanding the mechanisms promoting changes in firing mode both intrathalamically (Destexhe et al., 1993; Wang and Rinzel, 1993) and on the cortical level (Wallenstein, 1993a, b). Computer simulations can be useful in such instances in that they may allow one to manipulate specific properties of a cell or circuit with greater detail and stability than may be possible empirically.

APPENDIX

In the simulations reported here, all variables have the following units unless otherwise stated: 1) voltage is in mV; 2) time is in ms; 3) conductance is in $\mu S/cm^2$; 4) capacitance is in nF; 5) current is in nA; 6) concentration is in M; and 7) volume = 1.

Rate functions

$I_{Na(fast)}$:

$$I_{Na(fast)} = \bar{g}_{Na(fast)} m^3 h\,(V - V_{Na(fast)}), \tag{7}$$

where $V_{Na(fast)} = 45$ mV, $\bar{g}_{Na(fast)} = 25\ \mu S$, and

$$\begin{aligned} \alpha_m(V) &= \frac{0.091(V + 38)}{1 - \exp[-(V + 38)/5]} \\ \beta_m(V) &= \frac{-0.062(V + 38)}{1 - \exp[(V + 38)/5]} \\ \alpha_h(V) &= 0.016 \exp[(-55 - V)/15] \\ \beta_h(V) &= \frac{2.07}{\exp[(17 - V)/21] + 1}. \end{aligned} \tag{8}$$

$I_{K(DR)}$:

$$I_{K(DR)} = \bar{g}_{K(DR)} m^4 (V - V_{K(DR)}), \tag{9}$$

where $V_{K(DR)} = -105$ mV, $\bar{g}_{K(DR)} = 10\ \mu S$, and

$$\begin{aligned} \alpha_m(V) &= \frac{0.01(-45 - V)}{\exp[(-45 - V)/5] - 1} \\ \beta_m(V) &= 0.17 \exp[-50 - V/0)] \end{aligned} \tag{10}$$

I_{Ts}:

The slow low-threshold Ca^{2+} current (Huguenard and Prince, 1992) was modeled using the Goldman-Hodgkin-Katz constant field equation

$$I_T = P_T m^2 h z^2 \frac{EF^2}{RT} \frac{[Ca^{2+}]_i - [Ca^{2+}]_o \exp(-zFE/RT)}{1 - \exp(-zFE/RT)}, \tag{11}$$

where $z = 2$ is the valence of Ca^{2+}, $P_T = 40 \times 10^{-9}$ cm^3/s is the maximum permeability, $[Ca^{2+}]_o = 2$ mM, and $[Ca^{2+}]_i$ is initially set 50 nM. The constants $R = 8.315\ JK^{-1}M^{-1}$ (gas constant), $T = 273.16 + t$(°celsius) (temperature on the Kelvin scale), and $F = 9.648 \times 10^4$ C M^{-1} (Faraday's constant). The rate functions were described by

$$\begin{aligned} m_\infty(V) &= 1/\{1 + \exp[-(V + 50)/7.4]\} \\ \tau_m(V) &= (1/\{\exp[-(V + 110)/17] + \exp[(V + 9)/15]\} + 1) \\ h_\infty(V) &= 1/\{1 + \exp[(V + 78)/5]\} \\ \tau_h(V) &= 90. \end{aligned} \tag{12}$$

I_L:

The L-type Ca^{2+} current was also modeled using the Goldman-Hodgkin-Katz constant field equation

$$I_L = P_T m^2 z^2 \frac{EF^2}{RT} \frac{[Ca^{2+}]_i - [Ca^{2+}]_o \exp(-zFE/RT)}{1 - \exp(-zFE/RT)}, \tag{13}$$

where $P_T = 80 \times 10^{-9}$ cm^3/s is the maximum permeability. The activation variable m was described by

$$\begin{aligned} \alpha_m(V) &= 1.6/\{1 + \exp[-0.072(V - 5)]\} \\ \beta_m(V) &= \frac{0.02(V - 1.31)}{\exp[(V - 1.31)/5.36] - 1}. \end{aligned} \tag{14}$$

$I_{K(Ca)}$:

$$I_{K(Ca)} = \bar{g}_{K(Ca)} m (V - V_{K(Ca)}), \tag{15}$$

where $V_{K(Ca)} = -105$ mV, $\bar{g}_{K(Ca)} = 10\ \mu S$, and

$$\alpha_m([Ca^{2+}]_i) = 48[Ca^{2+}]_i \qquad \beta_m([Ca^{2+}]_i) = 0.03. \tag{16}$$

I_{CAN}:

$$I_{CAN} = \bar{g}_{CAN} m (V - V_{CAN}), \tag{17}$$

where $V_{CAN} = -20$ mV, $\bar{g}_{CAN} = 0.2\ \mu S$, and

$$\alpha_m([Ca^{2+}]_i) = 20\,[Ca^{2+}]_i^2 \qquad \beta_m([Ca^{2+}]_i) = 0.002. \tag{18}$$

$I_{Na(P)}$:

$$I_{Na(P)} = \bar{g}_{Na(P)} m (V - V_{Na(P)}), \tag{19}$$

where $V_{Na(P)} = 45$ mV, $\bar{g}_{Na(P)} = 4.5$ nS, and

$$m_\infty(V) = 1/\{1 + \exp[(-49 - V)/5]\} \tag{20}$$

described the activation curve. The activation kinetics were assumed to be the same as those of $I_{Na(fast)}$ (French et al., 1990; McCormick and Huguenard, 1992).

$I_{K(A)}$:

$$I_{K(A)} = \bar{g}_{K(A)} (0.6\, m_1^4 h_1 + 0.4\, m_2^4 h_2)(V - V_{K(A)}), \tag{21}$$

where $V_{K(A)} = -105$ mV, $\bar{g}_{K(A)} = 1.5$ μS, and

$$m_{1\infty}(V) = 1/\{1 + \exp[-(V + 60)/8.5]\}$$

$$m_{2\infty}(V) = 1/\{1 + \exp[-(V + 36)/20]\}$$

$$\tau_{m1,2}(V) = 1/\{\exp[(V + 35.8)/19.7] + \exp[-(V + 79.7)/12.7]\} + 0.37$$

$$h_{1,2\infty}(V) = 1/\{1 + \exp[(V + 78)/6]\}$$

$$\tau_{h1}(V) = 1/\{\exp[(V + 46)/5] + \exp[-(V + 238.5)/37.5]\} \quad \forall V < -63 \text{ mV} \tag{22}$$

$$\tau_{h1}(V) = 19 \quad \forall V \geq -63 \text{ mV}$$

$$\tau_{h2}(V) = 1/\{\exp[(V + 46)/5] + \exp[-(V + 238.5/37.5]\} \quad \forall V < -73 \text{ mV}$$

$$\tau_{h2}(V) = 60 \quad \forall V \geq -73 \text{ mV}.$$

$I_{Na(leak)}$ and $I_{K(leak)}$:

$$I_{Na(leak)} = \bar{g}_{Na(leak)}(V - V_{Na(leak)}),$$
$$I_{K(leak)} = \bar{g}_{K(leak)}(V - V_{K(leak)}), \tag{23}$$

where $V_{Na(leak)} = 45$ mV, $\bar{g}_{Na(leak)} = 1$ nS, $V_{K(leak)} = -105$ mV, and $\bar{g}_{K(leak)} = 7$ nS.

Calcium buffering

The internal calcium concentration, $[Ca^{2+}]_i$, was calculated for a depth of 100 nm beneath the surface of the cell. A simple linear diffusion model was adopted to describe the time-dependent variation of this quantity (Traub et al., 1991; McCormick and Huguenard, 1992),

$$\frac{d[Ca^{2+}]_i}{dt} = \beta[Ca^{2+}]_i, \tag{24}$$

where β scales the rate of diffusion. A value of $\beta = 1$ was used in these simulations at 35°C. The discretized equation used to calculate internal calcium can be expressed as,

$$[Ca^{2+}]_{i_t} = [Ca^{2+}]_{i_{t-1}} + dt\left(\frac{-5.18 \times 10^{-3} I_L}{\text{area} \cdot \text{depth}} - \beta[Ca^{2+}]_{i_{t-1}}\right), \tag{25}$$

where -5.18×10^{-3} is a constant used to convert current (nA), time (ms), and volume (μm^3) into $[Ca^{2+}]_i$ ion concentrations.

This work was partially supported by National Institute of Mental Health National Training Program S T32 MH19116.

REFERENCES

Asanuma, C. 1989. Axonal arborations of a magnocellular basal nucleus input and their relation to the neurons in the thalamic reticular nucleus of rats. *Proc. Natl. Acad. Sci. USA.* 86:4746–4750.

Asanuma, C. 1992. Noradrenergic innervation of the thalamic reticular nucleus: A light and electron microscopic immunohistochemical study in rats. *J. Comp. Neurol.* 319:299–311.

Avanzini, G., M. De Curtis, F. Panzica, and R. Spreafico. 1989. Intrinsic properties of nucleus reticularis thalami neurons of the rat studied *in vitro*. *J. Physiol.* 416:111–122.

Bal, T., and D.A. McCormick. 1993. Mechanisms of oscillatory activity in guinea-pig nucleus reticularis thalami *in vitro*: a mammalian pacemaker. *J. Physiol.* 468:669–691.

Crunelli, V., and N. Leresche. 1991. A role for $GABA_B$ receptors in excitation and inhibition of thalamocortical cells. *Trends Neurosci.* 14: 16–21.

Deschênes, M., A. Madariaga-Domich, and M. Steriade. 1985. Dendrodendritic synapses in the cat reticularis thalami nucleus: A structural basis for thalamic spindle synchronization. *Brain Res.* 334:165–168.

Destexhe, A., D.A. McCormick, and T.J. Sejnowski. 1993. A model for 8–10 Hz spindling in interconnected thalamic relay and reticularis neurons. *Biophys. J.* 65:2473–2477.

Huguenard, J.R., D.A. Coulter, and D.A. Prince. 1991. A fast transient potassium current in thalamic relay neurons: kinetics of activation and inactivation. *J. Neurophysiol.* 66:1304–1315.

French, C.R., P. Sah, K.J. Buckett, and P.W. Gage. 1990. A voltage-dependent persistent sodium current in mammalian hippocampal neurons. *J. Gen. Physiol.* 95:1139–1157.

Hallanger, A.E., A.I. Levey, H.J. Lee, D.B. Rye, and B.H. Wainer. 1987. The origins of cholinergic and other subcortical afferents to the thalamus in the rat. *J. Comp. Neurol.* 262:105–124.

Harris, R.M. 1987. Axon collaterals in the thalamic reticular nucleus from thalamocortical neurons in the rat ventrobasal thalamus. *J. Comp. Neurol.* 258:397–406.

Hodgkin, A.L., and A.F. Huxley. 1952. A quantitative description of membrane current and its application to conduction and excitation in nerve. *J. Physiol.* 117:500–544.

Huguenard, J.R., O.P. Hamill, and D.A. Prince. 1988. Developmental changes in Na^+ conductances in rat neocortical neurons: appearance of a slowly inactivating component. *J. Neurophysiol.* 59:778–795.

Huguenard, J.R., and D.A. Prince. 1992. A novel T-type current underlies prolonged Ca^{2+}-dependent burst firing in GABAergic neurons of rat thalamic reticular nucleus. *J. Neurosci.* 12:3804–3817.

Jahnsen, H., and R.R. Llinás. 1984a. Electrophysical properties of guinea-pig thalamic neurones: an in vitro study. *J. Physiol.* 349:205–226.

Jahnsen, H., and R.R. Llinás. 1984b. Ionic basis for the electroresponsiveness and oscillatory properties of guinea-pig thalamic neurones in vitro. *J. Physiol.* 349:227–247.

Kay, A.R., and R.K.S. Wong. 1987. Calcium current activation kinetics in isolated pyramidal neurons of the CA1 region of the mature guinea-pig hippocampus. *J. Physiol.* 392:603–616.

Lavoie, B., and A. Parent. 1991. Serotoninergic innervation of the thalamus in primate: an immunohistochemical study. *J. Comp. Neurol.* 312: 1–18.

McCormick, D.A. 1989. Cholinergic and noradrenergic modulation of thalamocortical processing. *Trends Neurosci.* 12:215–221.

McCormick, D.A. 1992a. Neurotransmitter actions in the thalamus and cerebral cortex and their role in neuromodulation of thalamocortical activity. *Prog. Neurobiol.* 39:337–388.

McCormick, D.A. 1992b. Cellular mechanisms underlying cholinergic and noradrenergic modulation of neuronal firing mode in the cat and guinea-pig dorsal lateral geniculate nucleus. *J. Neurosci.* 12:278–289.

McCormick, D.A., and J.R. Huguenard. 1992. A model of the electrophysiological properties of thalamocortical relay neurons. *J. Neurophysiol.* 68:1384–1400.

McCormick, D.A., and D.A. Prince. 1986. Acetylcholine induces burst firing in thalamic reticular neurones by activating a potassium conductance. *Nature (Lond.)* 319:402–405.

McCormick, D.A., and D.A. Prince. 1988. Noradrenergic modulation of firingpatterns in guinea-pig and cat thalamic neurones in vitro. *J. Neurophysiol.* 59:978–996.

McCormick, D.A., and Z. Wang. 1991. Serotonin and noradrenaline excite GABAergic neurones of the guinea-pig and cat nucleus reticularis thalami. *J. Physiol.* 442:235–255.

Morison, R.S., and D.L. Bassett. 1945. Electrical activity of the thalamus and basal ganglia in decorticate cats. *J. Neurophysiol.* 8:309–314.

Mulle, C., A. Madariaga, and M. Deschênes. 1986. Morphology and electrophysiological properties of reticularis thalami neurons in cat: in vivo study of a thalamic pacemaker. *J. Neurosci.* 6:2134–2145.

Nuñez, A., F. Amzica, and M. Steriade. 1992. Intrinsic and synaptically generated delta (1–4 Hz) rhythms in dorsal lateral geniculate neurons and their modulation by light-induced fast (30–70 Hz) events. *Neuroscience.* 51:269–284.

Partridge, L.D., and D. Swandulla. 1988. Calcium-activated non-specific cation channels. *Trends Neurosci.* 11:69–72.

Pinault, D., and M. Deschênes. 1992. Voltage dependent 40 Hz oscillations in rat reticular thalamic neurons in vivo. *Neuroscience.* 51:245–258.

Steriade, M., and M. Deschênes. 1984. The thalamus as a neuronal oscillator. *Brain Res. Rev.* 8:1–63.

Steriade, M., L. Domich, and G. Oakson. 1986. Reticularis thalami neurons revisited: activity changes during shifts in states of vigilance. *J. Neurosci.* 6:68–81.

Steriade, M., L. Domich, G. Oakson, and M. Deschenes. 1987. The deafferented reticular thalamic nucleus generates spindle rhythmicity. *J. Neurophysiol.* 57:260–273.

Steriade, M., P. Gloor, R.R. Llinás, F.H. Lopes da Silva, M.M. Mesulam. 1990. Basic mechanisms of cerebral rhythmic activities. *Electroenceph. Clin. Neurophys.* 76:481–508.

Steriade, M., and R. Llinás. 1988. The functional states of the thalamus and the associated neuronal interplay. *Physiol. Rev.* 68:649–742.

Traub, R.D., R.K.S. Wong, R. Miles, and H. Michelson. 1991. A model of a CA3 hippocampal pyramidal neuron incorporating voltage-clamp data on intrinsic conductances. *J. Neurophysiol.* 66:635–650.

von Krosigk, M., T. Bal, and D.A. McCormick. 1993. Cellular mechanisms of a synchronized oscillation in the thalamus. *Science (Wash. DC).* 261: 361–364.

Wallenstein, G.V. 1993a. Spatial, temporal, and global mode entropy in a thalamo-cortical network. *Int. J. Bifurcation Chaos.* In press.

Wallenstein, G.V. 1993b. Spatial mode dynamics of a thalamo-cortical network. *In* SPIE Proceedings on Chaos in Biology and Medicine, W.L. Ditto, Editor. Vol. 2036, pp 301–312.

Wang, X.J., and J. Rinzel. 1993. Spindle rhythmicity in the reticularis thalami nucleus: Synchronization among mutually inhibitory neurons. *Neuroscience.* 53:899–904.

Yamada, W.M., C. Koch, and P. Adams. 1989. Multiple channels and calcium dynamics. *In* Methods in Neuronal Modeling: From Synapses to Networks. C. Koch and I. Segev, Editors. MIT Press, Cambridge, MA. 97–133.